



HAL
open science

Elongation mechanism of the ion shaping of embedded gold nanoparticles under swift heavy ion irradiation

T.H.Y. Vu, C. Dufour, V. Khomenkov, A.A. Leino, F. Djurabekova, K. Nordlund, P.-E. Coulon, G. Rizza, M. Hayoun

► To cite this version:

T.H.Y. Vu, C. Dufour, V. Khomenkov, A.A. Leino, F. Djurabekova, et al.. Elongation mechanism of the ion shaping of embedded gold nanoparticles under swift heavy ion irradiation. Nuclear Instruments and Methods in Physics Research Section B: Beam Interactions with Materials and Atoms, 2019, 451, pp.42-48. 10.1016/j.nimb.2019.04.067 . hal-02272399

HAL Id: hal-02272399

<https://hal.science/hal-02272399>

Submitted on 22 Oct 2021

HAL is a multi-disciplinary open access archive for the deposit and dissemination of scientific research documents, whether they are published or not. The documents may come from teaching and research institutions in France or abroad, or from public or private research centers.

L'archive ouverte pluridisciplinaire **HAL**, est destinée au dépôt et à la diffusion de documents scientifiques de niveau recherche, publiés ou non, émanant des établissements d'enseignement et de recherche français ou étrangers, des laboratoires publics ou privés.



Distributed under a Creative Commons Attribution - NonCommercial 4.0 International License

Elongation mechanism of the ion shaping of embedded gold nanoparticles under swift heavy ion irradiation

T. H. Y. Vu¹, C. Dufour², V. Khomenkov^{2,4}, A. A. Leino³, F. Djurabekova³, K. Nordlund³, P.-E. Coulon¹, G. Rizza¹, and M. Hayoun^{1*}

¹Laboratoire des Solides Irradiés, École Polytechnique, CNRS, CEA, Université Paris-Saclay, F-91128 Palaiseau Cedex, France

²CIMAP-ENSICAEN-CEA-CNRS, Université de Caen, bd H. Becquerel, Boîte Postale 5133, F-14070 Caen Cedex 5, France

³Helsinki Institute of Physics and Department of Physics, University of Helsinki, PO Box 43, Helsinki, FI-00014, Finland

⁴ Institute for Nuclear Research, 47 Nauky Ave., Kiev 03680, Ukraine.

ABSTRACT

The elongation process under swift heavy ion irradiation (74 MeV Kr ions) of gold NPs, with a diameter in the range 10-30 nm, and embedded in a silica matrix has been investigated by combining experiment and simulation techniques: three-dimensional thermal spike (3DTS), molecular dynamics (MD) and a phenomenological simulation code specially developed for this study. 3DTS simulations evidence the formation of a track in the host matrix and the melting of the NP after the passage of the impinging ion. MD simulations demonstrate that melted NPs have enough time to expand after each ion impact. Our phenomenological simulation relies on the expansion of the melted NP, which flows in the track in silica with modified (lower) density, followed by its recrystallization upon cooling. Finally, the elongation of the spherical NP into a cylindrical one, with a length proportional to its initial size and a width close to the diameter of the track, is the result of the superposition of the independent effects of each expansion/recrystallization process occurring for each ion impact. In agreement with experiment, the simulation shows the gradual elongation of spherical NPs in the ion-beam direction until their widths saturate in the steady state and reach a value close to the track diameter. Moreover, the simulations indicate that the expansion of the gold NP is incomplete at each ion impact.

I. INTRODUCTION

The appearance of large accelerator facilities in early 1980s opened the door to the exploration of the ion-matter interaction in the until then unexplored MeV-to-GeV energy region. Since then, most of all two effects focused the attention of the swift heavy ion (SHI) community creating a widespread scientific excitement and in turn a copious literature: the ion hammering and the ion shaping. The ion hammering was discovered in 1983 by Klaumünzer [1]. During this process, sample dimensions are observed to grow perpendicular to the ion beam whereas those parallel to the ion beam are observed to shrink. The ion shaping was discovered by d'Orléans *et al.* in 2003 [2], in the wake of the interest sparked by nanosciences. During this process, metallic nanoparticles (NPs) embedded within an amorphous matrix are observed to become prolate, i.e. their major axis becomes oriented parallel to the incident ion direction. The ion hammering mechanism is nowadays well understood and quantitatively described by the *Effective-Flow Temperature Approach* (EFTA) model [3]. On the other hand, a consistent description of the ion-shaping phenomenon is still lacking. The first rational model was proposed in 2004 by Roorda *et al.* using Au@SiO₂ core-shell NPs as a model system [5]. Here, the melting of the NPs is not considered and the deformation of a radiation-softened Au NP is assumed to be driven by the ion hammering of silica matrix generating an in-plane mechanical stress.

However, in 2006 Klaumünzer demonstrated that this stress (of the order of 100-300 MPa) is too low to induce the deformation of a solid NP [6], that must play an active role. The necessity for the NP to be in a liquid phase to be shaped was confirmed in 2012 by Dufour *et al.* [7] using a thermal spike model implemented in three dimensions and optimized for nanocomposite materials. This is known as the three-dimensional thermal spike (3DTS) code. In particular, these simulations showed the existence of an intermediate phase where the NP is only partially molten. This is, a phase where a solid core is surrounded by a liquid shell. In a companion paper published in 2012 Rizza *et al.* [8] showed that the ion shaping of a NP is driven by its degree of melting such that four deformation pathways can be experimentally observed: i) vaporized NPs (0-10 nm) maintain their spherical morphology. ii) Completely molten NPs (10-30 nm) deform into nanorods and subsequently into nanowires for larger fluences. iii) Partially molten NPs (30-70 nm) are first transformed into faceted NPs that, in turn, become nanowires, for larger fluences. Finally, iv) NPs larger than about 60-70 nm do not melt and show a very low deformation rate. Although, the paper of Dufour *et al.* [7] represents an advance in the understanding of the ion-shaping mechanism, it is nonetheless limited to the simulation the heat

exchange between the electronic to the atomic subsystems. Otherwise stated, to elucidate the fundamentals of the shaping process the transport of matter must be taken into account. This gap was bridged in 2014 by Leino *et al.* [9] using molecular dynamics (MD) simulations coupled with the two temperatures model in the MD-TTM scheme [10-11]. In this approach, initial atomic velocities are randomly assigned using the simulated maximum lattice temperature. These simulations suggest that the elongation of the NP remains spatially confined to the core of the molten ion track in silica and it is not a consequence of the ion-hammering effect or of any diffusion-like processes. Experimentally, similar conclusions have been reached by Amekura *et al.* [12] and d'Orléans *et al.* [13] whose results indicate that the deformations occur in a fluence domain not explained by the ion-hammering effect.

Available experiments indicate that the ion-shaping process is not observed if the NPs are embedded in radiation-resistant matrix [14-15], but only if they are embedded in an amorphous matrix [5, 16-19]. In addition, it has been demonstrated that the ion-track formation is a necessary condition for the observation of the elongation of the NPs [20-21]. Finally, the agreement between SAXS measurements and MD simulations indicates that in silica the ion track has an underdense core/overdense shell structure and that a potential mechanism for the elongation should be the flow of the NP into the underdense core of the ion track in surrounding silica matrix [20].

Undeniably, the use of MD simulations paved the way to a better understanding of the ion-shaping process, however its intrinsic time and size limitations prevent to follow the complete deformation history of a NP of arbitrary dimension. This is clearly evidenced in Leino simulations where the largest NP, 12 nm in diameter, is observed to evolve toward a lemon-like prolate shape (after 12 ion impacts) without reaching the expected rod-like configuration. Furthermore, as aforementioned, this size (12 nm) is at the boundary between two deformation regions [8]: i) NPs smaller than 10 nm which vaporize during the thermal spike duration and are observed to remain spherical in shape, and ii) NPs in the range 10-30 nm which completely melt during the thermal spike duration and are observed to transform into prolate (nanorods and nanowires) structures.

The aim of the present work is to give a contribution to the understanding of the ion-shaping mechanism of gold NPs embedded in a silica matrix by performing the simulation of the elongation process in the regime where a NP is completely molten during irradiation, i.e. in the range 10 to 30 nm. To reach this objective we developed a phenomenological simulation code.

The code is based on the mechanism observed by Leino *et al.* in their MD simulations [9]. The basic ingredient of the code is the expansion/recrystallization of the gold NP taking place at each impact of the incident ion, ignoring the stages leading to this state. The code is sufficiently light such that it is possible to run with a realistic computing time and its outcome provides a qualitative description of the overall morphological transformation of the NP from the sphere to the rod/wire configuration.

The manuscript is organized as follows. We first present the experimental and simulation techniques used to investigate the ion shaping of gold NPs (Section II). All the results obtained are reported and discussed in Section III.

II. METHODS

II.A. Sample preparation and irradiation

Electron beam lithography (EBL) has been used to fabricate arrays of spherical gold (Au) NPs embedded within a dielectric silica (SiO₂) matrix onto a silicon substrate. The fabrication procedure is described in [22]. High-angle annular dark-field (HAADF) micrograph of Figure 1a shows the as-prepared sample. The initial configuration is composed of spherical Au NPs (30±2 nm) sandwiched between two silica (SiO₂) layers. Successively, samples have been irradiated in GANIL (Caen, France) with 74 MeV Kr ions under constant flux (5×10⁹ cm⁻² s⁻¹) for fluences up to 5×10¹⁴ cm⁻² (figures 1b-d). Irradiations have been performed at room temperature and normal incidence with respect to the sample surface. SRIM2008 code [23] has been used to calculate the electronic (S_e) and nuclear (S_n) stopping powers: $S_e^{\text{SiO}_2} = 9.2 \text{ keV.nm}^{-1}$, $S_n^{\text{SiO}_2} = 4 \times 10^{-2} \text{ keV nm}^{-1}$, $S_e^{\text{Au}} = 25.6 \text{ keV.nm}^{-1}$, $S_n^{\text{Au}} = 0.17 \text{ keV nm}^{-1}$. Samples have been observed in cross-sectional and at medium magnification (×50k to ×120k) using a JEOL 2010F electron microscope operating at 200 kV.

II.B. 3D thermal spike simulation (3DTS) [7]

The 3D thermal spike (3DTS) model, [7], is an implementation in three dimensions and for real nanocomposite materials of the existing two dimensional i-TS models [10]. In particular, the 3DTS code allows simulating the thermal evolution, which follows the interaction of SHI with the matter, of embedded NPs of any shape and any orientation within the host matrix, where i-TS code only allows coaxial cylindrical configurations to be simulated. Moreover, following the work of Daraszewicz and Duffy [24], the model has been extended to insulators and explicitly takes into account the diffusion of heat through the matrix/metal interface. For the interested

reader, all the parameters that were used in the calculations of section III.B can be found in Ref [7].

II.C. Molecular Dynamic (MD) simulation of the NP thermal expansion

The energy deposited by the impinging SHI into the NP is rapidly transferred from the electronic to the atomic subsystem in the form of heat (see section II.B). Thus, MD simulation is used to estimate the thermal-expansion velocity of gold spherical NPs in vacuum with a diameter in the range 4 to 10 nm when the temperature is increased from 300 K up to a temperature (1500 K) greater than the melting point. Dataset is then extrapolated to larger NP sizes up to 30 nm. Here, Au-Au interactions are described using an empirical n-body potential [25] of the tight-binding type [26-27] that satisfactorily reproduces their physical properties. The simulation cell is cubic and large enough to follow the expansion of one spherical NP. The computations were carried out in two successive MD runs by integrating the equations of motion with the Verlet algorithm [28] and a time step of 2×10^{-15} s.

The first MD run, performed in the microcanonical ensemble, allows the equilibration of the NP at a temperature around 300 K. The second MD run is used to estimate the time necessary for the complete expansion of the NP. Here, the system is initially maintained at 300 K and then progressively heated, with incremental steps of 120 K, up to a temperature of ~ 1500 K (melting point = 1323 K). At each step, the temperature is controlled by using the Nosé thermostat [29-30]. The new temperature is maintained during 12 to 30×10^{-15} s, depending on the total heating time chosen to reach the maximal temperature. In order to equilibrate the system at the maximal temperature, the system is simulated during few picoseconds to few hundred picoseconds, depending on the NP size.

III. RESULTS AND DISCUSSION

III.A. Experiment

The elongation process is shown in Figures 1b-d). Spherical NPs are first transformed into prolate ellipsoids at 5×10^{13} cm⁻² (Fig.1b) and sequentially into nanorods (1×10^{14} cm⁻², Fig. 1c) whose length and width are 100 ± 4 nm and 14 ± 2 nm, respectively. It is worth mentioning that, as the ion-shaping takes place at almost constant volume and the size dispersion of the as-prepared NPs is narrow, the elongation rate is nearly the same for all the NPs [22]. Finally at 5×10^{14} cm⁻² they are further elongated into nanowires (Fig. 1d), of length 225 ± 6 nm and width 9 ± 1 nm. Here, for the sake of clarity the terms *nanorods* and *nanowires* are here used to distinguish NPs of different aspect ratio.

III.B. Spatiotemporal evolution of the lattice temperature in both silica and gold NP

In this section, we analyze the results of 3DTS simulations corresponding to the deformation of spherical gold NPs into rod-shaped NPs. The initial diameter of the NPs has been considered in the range between 10 and 30 nm.

First, we consider the spatiotemporal evolution of the temperature within the silica matrix during the impact of a 74 MeV Kr ion passing through the center of the NP. This evolution is shown in figure 2a-b along the irradiation axis, i.e. the z-axis, for both electronic and lattice subsystems. 3DTS simulations indicate that the silica is heated 10^{-16} s after the impact and before the heating of the gold NP (10^{-13} s). Otherwise stated, for times shorter than about 3×10^{-13} s a cylindrical hot region, the ion track, is formed within the silica matrix around the ion trajectory while the lattice temperature within the metallic NP does not change noticeably, such that the NP remains in the solid state. For silica, the hottest part of the track is located at its center and the temperature radially decreases towards the edges. Its diameter has been estimated to be about 11 nm by considering the region where the temperature is larger than the melting point of silica ($T=1983$ K). For times larger than about 10^{-13} s, the heating/melting of the metallic NP modifies the temperature profile of the ion track in silica in the vicinity of its surface. This is shown in figure 2c where the temperature profile of the ion track in silica is given as a function of both the time and the distance from the NP surface, $z-r_p$. This profile does not depend on the size of the embedded NP in the range 10 to 30 nm [8]. The largest temperature for the track in silica ($T=12 \times 10^3$ K) is measured close to the NP surface, i.e. for $z-r_p=0.5$ nm, and decreases as far as moving away from it. The effect of the surface becomes negligible for distances larger than about 5 nm. After the initial thermal burst, the ion track evolves toward a stationary state wherein the temperature is always higher than the silica melting point. This steady state lasts for about 10 ps.

The spatiotemporal evolution of the temperature within the NPs is given in figure 3 for four sizes of the NP, i.e. $d = 2 r_p = 12, 16, 20$ and 24 nm. In all cases, the temperature evolves from 300 K up to about 2000-3000 K, which is larger than the melting point of bulk gold (1323 K). Thus, all the NPs become molten after the passage of the SHI. Simulations indicate that the heating of the NP occurs from the surface toward the core of the NP.

A phenomenological explanation can be given by considering the electronic thermal conductivity (\mathbf{k}_e) and the value for the electron-phonon coupling constant (\mathbf{g}) for both silica and metallic NPs. Silica presents low values of \mathbf{k}_e and high values of \mathbf{g} . Thus, the energy deposited by the impinging ions remains spatially localized within the ion trajectory where it is rapidly thermalized. This results in the formation of an ion track that is narrow and hot. Conversely, gold

presents high values of k_e and low values of g . Thus, owing to the weak coupling between the electronic and lattice subsystems, the electronic temperature rapidly increases, while the lattice temperature is only slightly affected. When gold NPs are confined within a silica matrix an interesting effect is observed. Indeed, the energy deposited to the electrons of the metallic particle is swiftly smeared out toward the Au/SiO₂ interface. Here, the interfacial thermal resistance favors the formation of a hot silica layer. The heat is then reflected back (it diffuses) to the center of the NP.

Owing to this indirect-heating mechanism, we estimated the time necessary to reach the molten phase at different positions within the NP from the center ($z = 0$) to its surface ($z = r_p = d/2$). In all cases, the heating is faster at the surface of the NP. For instance, for a NP of size $d = 2 r_p = 12$ nm, the heating time is shifted from 0.11 ps at the edge ($z = 5.5$ nm) to 0.8 ps at the core ($z = 0.5$ nm). At the same time, the melting of the core is also retarded when the NP size is increased. For instance, the heating time is 0.8 ps for a NP of size $d = 2 r_p = 12$ nm and 3 ps for a NP of size $d = 2 r_p = 24$ nm.

To summarize this section, 3DTS simulations indicate that both the track in silica and the gold NP (in the range 10 to 30 nm) melt and that they are simultaneously in the liquid state during about 50 ps (see Fig. 4 in ref. 8). These results of the solid-liquid transformations will be used in the phenomenological simulation of section III.D. After the ion impact, NPs quickly melt and then expand to reach the density of liquid gold. 3DTS simulation describes the thermal state of the system but does not give any information on the corresponding atomic displacements and particularly on the NP expansion. This information can be obtained through the MD simulation described in the next section.

III.C. Thermal expansion of a molten gold NP

MD simulations (computational details are given in section II.C) have been performed to study the thermal expansion of gold NPs surrounded by vacuum. Let us consider a NP undergoing a temperature increase from 300 K up to a chosen temperature of 1500 K larger than its melting point (1323 K). The goal is to determine the time for the complete expansion of the NP for diameters in the range 10-30 nm. This time must be compared to the time during which the track and the NP are simultaneously in the liquid state, i.e. 50 ps (see section III.B). If the thermal expansion lasts less than 50 ps the NP can expand completely, otherwise the expansion will be only partial.

In the previous section, we have shown that the heating time to reach the molten phase is function of both the position within the NP as well as its dimension. In particular, the melting of

the core of the NP is retarded with respect to its surface, which melts first. To check if this delay plays a role in the expansion process, MD simulations have been performed considering the volume expansion when the heating time is varied. Figure 4 shows the time evolution of the volume of a NP of 4 nm when the heating time is increased from 0 to 0.8 ps.

In response to the pressure change induced by the heating, the NP quickly expands and its volume first reach a maximum value and then damps oscillates around the equilibrium value. The shorter heating time, the faster the pressure change and the greater the maximum volume and the oscillation amplitudes. Moreover, the velocity of the NP expansion only slightly depends on the heating time, where only the amplitude of the oscillations changes. In conclusion, the heating time is short enough such that it has solely a slight effect on the expansion rate of the NP.

In order to estimate the expansion time as a function of the NP size, MD simulations have been carried out for spherical gold NP with a diameter ranging from 4 to 10 nm. The expansion time is determined as the time required to reach the value of the equilibrium volume before the first oscillation in Fig. 4. This value is reported in figure 5 as a function of the NP size. As time required for MD simulations increases with the dimension of the considered NP, the expansion time for NPs larger than 10 nm has been obtained by linear extrapolation of the simulated values obtained for NPs from 4 to 10 nm.

The main result is that the expansion time of NPs with a diameter less than 30 nm never exceeds 9 ps, which is much lesser than the time where both the silica track and the gold NP are simultaneously in the liquid state, i.e. 50 ps (see section III.B).

In conclusion, the MD simulations demonstrated that gold NPs ranging between 10 and 30 nm have enough time to fully expand after each ion impact, and that neither the heating time nor the expansion time are relevant parameters for the phenomenological model of the ion shaping of gold NPs developed in the next section.

III.D. Phenomenological model for the NP elongation under SHI irradiation

The two necessary conditions for the ion shaping are i) the formation of an ion track with modified (lower) density region in the host matrix and ii) the melting of the NP after the passage of the impinging ion (cf. section I). Our 3DTS simulations (Section III.B) have shown that both these conditions are satisfied in the case of gold NPs embedded within a silica matrix irradiated with 74 MeV Kr ions.

We now describe our phenomenological model, which allows the simulation of the elongation process for NPs larger than 10 nm. The model is based on the expansion of the gold NP during the melting phase and its recrystallization upon cooling, ignoring the stages leading to

these states. In the previous sections, we have shown that the melting of the NP is so fast that the molten phase initially keeps the density of the solid one before the expansion leads to the density of the liquid phase. On the other hand, in the surrounding silica matrix, the track is a molten cylindrical region presenting a reduced density (compared to solid), which can accommodate the thermal expansion of the gold NP. This reduced density region can be larger than the simple underdense core. [31]. Thus, during the time where the NP and the track in silica are simultaneously in the liquid phase, the molten NP can flow into the track. The difference of volume of the NP between the solid and liquid states, ΔV , is obtained by using the experimental densities of gold in these two phases. This value corresponds to the complete expansion of the NP and gives the volume of gold, which flows into the track in silica at each ion impact. After its expansion, the NP cools and recrystallizes, keeping the general shape it had in the liquid state and recovering the solid density by contracting. The recrystallization stage was previously simulated by Leino *et al.* on nanosecond (ns) timescales, [9]. In agreement with the experimental results, MD simulations showed that the NP evolved towards a polycrystalline state. However, simulation of full recrystallization was not achieved due to the limited time scale of the simulation.

The final result of the expansion/recrystallization process is the flow of a volume ΔV of gold within the ion track in silica. As the cylindrical track is symmetrically developed with respect to the equator of the NP, the flow of matter takes place on both sides of the NP. The expansion/recrystallization process is repeated for each ion impact, which corresponds to a simulation step. Two approximations are made in the present model: i) the resistance of the track against the NP expansion is not taken into account, and ii) for simplicity, all incident ions go through the NP center, whereas it is not the case experimentally. Furthermore, for the irradiation flux used in these experiments with SHI, i.e. 3×10^9 ions $\text{cm}^{-2} \text{s}^{-1}$, the elapsing time between two successive ion impacts with the NP is about ~ 100 s, which is orders of magnitude larger than the time necessary to relax the system toward recrystallization. Thus, the final state of the gold NP is the result of the superposition of the independent effects of each ion impact. If the irradiation time is long enough, the spherical NP is transformed into a cylindrical one with a length proportional to its initial size and a width close to the diameter of the track in silica [32].

III.E. Comparing phenomenological simulation results with experimental data

In this section, the results of our phenomenological simulation, based on the repetition of the expansion/recrystallization scenario, are presented for NPs with a diameter ranging between 10 and 30 nm.

Figure 6 shows the morphological evolution of a spherical NP, with a 16 nm initial diameter, toward a cylindrical nanorod aligned along the beam direction (indicated by the arrow). The simulation was performed considering a track having a diameter of 10 nm, which corresponds to the experimental value obtained for irradiation with 74 MeV Kr ions in silica [8]. Upon irradiation, the NP elongates along the trajectory of the ion while it shrinks in the normal direction. As abovementioned, the irradiation time, or fluence, is not directly given in the simulation but is related to the number of incident ions impacting the NP at its center. We observe that after the first impact (ion 1) the flow of the metallic species into the ion track in silica, which is associated to the expansion/recrystallization process, results in the formation of two small protrusions at the poles of the NP. The following impacts gradually deform the NP until its small diameter reaches a value close to the width of the track. This defines the end of the shaping process and the reaching of a steady-state condition. It is worth noticing that our simulation does not take into account neither the fragmentation nor the dissolution of the prolate structure once it reaches the steady state [33].

Elongation process can be investigated by considering the aspect ratio W/L between the length (L) and width (W) of the NPs. Thus, all spherical NPs are on a line of unitary slope, i.e. $W/L=1$. Figure 7a shows the simulation results for NPs with a diameter in the range between 17 to 26 nm. Clearly, when increasing the number of ion impacts the width-to-length ratio (W/L) approaches the steady state value to (W_c/L) , which scales with the initial NP size. According to available experimental results, [32], the threshold value for deformation, W_c , and the reaching of the steady state for the ion-shaped NPs is observed at about 10 nm. This value is related to the track diameter in silica [33]. Although qualitative, the correspondence with experimental results is quite straightforward, Figure 7b. As for the simulation counterpart, the experimental width-to-length ratio (W/L) for non irradiated NPs lies on a line of slope close to one. As expected, the simulated saturation is obtained after much less ion impacts than in the experiment. For instance in the case of a 20 nm NP, the simulation requires only 20 impacts whereas an experimental fluence of 10^{14} cm^{-2} , or 300 impacts, is necessary. This discrepancy is due first to an expansion velocity of the NP too high in the simulation, since a complete expansion is considered at each ion impact. This means that the silica matrix strongly resists the NP expansion. Hence, we can fairly conclude that the NP expansion is incomplete at each impact. The ratio of the numbers of ion impacts – simulated/experimental – necessary for the saturation leads to a rough estimation of an effective expansion rate ($\approx 7\%$). This hypothesis is supported by the MD simulation performed by Leino *et al.* where the silica surrounding is explicitly modeled [34]. Indeed, the expansion

process ended 20 ps after the ion impact upon the freezing of the silica track, indicating that the silica matrix resists to the expansion, which in turn remains incomplete. Another contribution to the erroneous acceleration of the NP expansion could be the fact considering only ion impacts passing through the NP center.

IV. CONCLUSION

The mechanism of elongation, under SHI irradiation, of metallic NPs embedded in a host matrix has been elucidated. First, the two necessary conditions for the elongation are the formation of a track in the host matrix with modified lower density and the melting of the NP after the passage of the impinging ion. We have shown that these conditions are satisfied for the irradiation with 74 MeV Kr ions of gold NPs, with a diameter ranging between 10 and 30 nm, and embedded within a silica matrix.

The melted gold NP expands and then cools and recrystallizes, keeping the general shape it had in the liquid state. The final result of the expansion/recrystallization process is the flow of a volume of gold within the track in silica. We have developed a phenomenological simulation code, which is based on the repetition of the expansion/recrystallization scenario at each ion impact passing through the NP center, ignoring the intermediate stages.

Our simulations qualitatively account for the elongation of a gold spherical NP into a cylindrical one in the direction of the ion beam and the shrinking of its volume toward a saturation width, which is close to the diameter of the track in silica. The simulations also show that the silica matrix strongly resists the NP expansion and that this expansion is thus incomplete at each ion impact. Work is in progress to improve the modeling by introducing both partial thermal expansion upon heating and by taking into account for off-axis ion impacts.

References

- [1] S. Klaumünzer, G. Schumacher, Phys. Rev. Lett. **51**, 1987 (1983).
Dramatic growth of glassy Pd₈₀Si₂₀ during heavy-ion irradiation.
- [2] C. D'Orléans, J. P. Stoquert, C. Estourns, C. Cerruti, J. J. Grob, J. L. Guille, F. Haas, D. Muller, M. Richard-Plouet, Phys. Rev. B **67**, 220101 (2003).
Anisotropy of Co nanoparticles induced by swift heavy ions.
- [3] H. Trinkaus, Nucl. Instr. and Meth. in Phys. Res. B **146** 204 (1998).
Dynamics of viscoelastic flow in ion tracks: origin of plastic deformation of amorphous materials.
- [4] J. D. Eshelby, Proceedings of the Royal Society of London. Series A, Mathematical and Physical Sciences Vol. **241**, 376 (1957).
The determination of the elastic field of an ellipsoidal inclusion, and related problems.
- [5] S. Roorda, T. van Dillen, A. Polman, C. Graf, A.M. Vredenberg, A. van Blaaderen, B. Kooi, Adv. Mater. **16**, 235 (2004).
Aligned gold nanorods in silica made by ion irradiation of core-shell colloidal particles.
- [6] S. Klaumünzer, Nucl. Instr. and Meth. in Phys. Res. B **244**, 1 (2006).
Modification of nanostructures by high-energy ion beams.
- [7] C. Dufour, V. Khomenkov, G. Rizza, M. Toulemonde, J. Phys. D Appl. Phys. **45**, 065302 (2012).
Ion-matter interaction: the three-dimensional version of the thermal spike model. Application to nanoparticle irradiation with swift heavy ions.
- [8] G. Rizza, P.-E. Coulon, V. Khomenkov, C. Dufour, I. Monnet, M. Toulemonde, S. Perruchas, T. Gacoin, D. Mailly, X. Lafosse, C. Ulysse and E. A. Dawi, Phys. Rev. B **86**, 035450 (2012).
Rational description of the ion-beam shaping mechanism.
- [9] A. A. Leino, O. H. Pakarinen, F. Djurabekova, K. Nordlund, P. Kluth, M. C. Ridgway, Mat. Res. Lett. **2**, 37 (2014).
Swift heavy ion shape transformation of Au nanocrystals mediated by molten material flow and recrystallization.
- [10] M. Toulemonde, W. Assmann, C. Dufour, A. Meftah, F. Studer, C. Trautmann, Mat. Fys. Med. Kong. Dan. Vid. Selsk **52**, 263 (2006).
Experimental Phenomena and Thermal Spike Model Description of Ion Tracks in Amorphisable Inorganic Insulators.
- [11] N.A. Medvedev, A.E. Volkov, N.S. Shcheblanov, B. Rethfeld, Phys. Rev. B **82**, 125425 (2010).
Early stage of the electron kinetics in swift heavy ion tracks in dielectrics.
- [12] H. Amekura, S. Mohapatra, U.B. Singh, S.A. Khan, P.K. Kulriya, N. Ishikawa, N. Okubo, D.K. Avasthi, Nanotechnology, **25**, 435301 (2014).

Shape elongation of Zn nanoparticles in silica irradiated with swift heavy ions of different species and energies: scaling law and some insights on the elongation mechanism.

- [13] C. D’Orleans, J. P. Stoquert, C. Estournes, J. J. Grob, D. Muller, C. Cerruti, F. Haas, Nucl. Instrum. Methods Phys. Res. B **225**, 154 (2004).
Deformation yield of Co nanoparticles in SiO₂ irradiated with 200 MeV ¹²⁷I ions.
- [14] C. Harkati Kerboua, M. Chicoine, S. Roorda, Nucl. Instr. Meth. B **269**, 2006 (2011).
Gold nanoparticles resist deformation by swift heavy ion irradiation when embedded in a crystalline matrix.
- [15] R. Giulian, F. Kremer, L. L. Araujo, D. J. Sprouster, P. Kluth, P. F. P. Fichtner, A. P. Byrne, M. C. Ridgway, Phys. Rev. B **82**, 113410 (2008).
Shape transformation of Sn nanocrystals induced by swift heavy-ion irradiation and the necessity of a molten ion track.
- [16] J. J. Penninkhof, T. van Dillen, A. Polman, C. Graf, A. van Blaaderen, Adv. Mater. **17**, 1484 (2005).
You have full text access to this content Angle-Dependent Extinction of Anisotropic Silica/Au Core/Shell Colloids Made via Ion Irradiation.
- [17] J. J. Penninkhof, T. van Dillen, C. Graf, A. van Blaaderen, A. M. Vredenberg, A. Polman, Nucl. Instr. and Meth. in Phys. Res. B, **242**, 523 (2006).
Anisotropic deformation of metallo-dielectric core–shell colloids under MeV ion irradiation.
- [18] J. J. Penninkhof, A. Moroz, A. van Blaaderen, A. Polman, J. Phys. Chem. C **112**, 4146 (2008).
Optical Properties of Spherical and Oblate Spheroidal Gold Shell Colloids.
- [19] J. J. Penninkhof, L. A. Sweatlock, A. Moroz, H. A. Atwater, A. van Blaaderen A. Polman, J. Appl. Phys. **103**, 123105 (2008).
Optical cavity modes in gold shell colloids.
- [20] P. Kluth, C. S. Schnohr, O. H. Pakarinen, F. Djurabekova, D. J. Sprouster, R. Giulian, M. C. Ridgway, A. P. Byrne, C. Trautmann, D. J. Cookson, K. Nordlund, M. Toulemonde, Phys. Rev. Lett. **101**, 175503 (2008).
Fine structure in swift heavy ion tracks in amorphous SiO₂.
- [21] T. Bierschenk, R. Giulian, B. Afra, M. D. Rodriguez, D. Schauries, S. Mudie, O. H. Pakarinen, F. Djurabekova, K. Nordlund, O. Osmani, N. Medvedev, B. Rethfeld, M. C. Ridgway, and P. Kluth, Phys. Rev. B **88**, 174111 (2013).
Latent ion tracks in amorphous silicon.
- [22] A. Slablab, T.J. Isotalo, J. Mäkitalo, L. Turquet, P.-E. Coulon, T. Niemi, C. Ulysse, M. Kociak, D. Maily, G. Rizza, M. Kauranen, Scientific Reports **6**, 37469 (2016).
Fabrication of Ion-Shaped Anisotropic Nanoparticles and their Orientational Imaging by Second-Harmonic Generation Microscopy.
- [23] F. Ziegler, J. P. Biersack, and M. D. Ziegler.
SRIM a version of the TRIM program, The Stopping and Range of Ions in Matter, 2008 (<http://www.srim.org>).

- [24] S.L.Daraszewicz, and D.M.Duffy, Nucl. Instr. Meth. **B** 269, 1646 (2010).
Extending the inelastic thermal spike model for semiconductors and insulators.
- [25] C. Rey-Losada, M. Hayoun, V. Pontikis, in *Materials Theory and Modeling*, J. Broughton, P. Bristowe, J. Newsam editors, MRS Symposia Proceedings No. 291, Materials Research Society, Pittsburgh, 1993, p. 549.
Monte Carlo and molecular dynamics validation of an N-body potential for Cu₃Au.
- [26] G. J. Ackland, V. Vitek, in *Atomistic simulation of materials: Beyond pair-potentials*, V. Vitek, D. J. Srolovitz editors, Plenum, New York, 1989, p. 193.
- [27] V. Rosato, M. Guillope, B. Legrand, Philos. Mag. A **59**, 321 (1989).
Thermodynamical and structural properties of f.c.c. transition metals using a simple tight-binding model.
- [28] L. Verlet, Phys. Rev. **159**, 98 (1967).
Computer “experiments” on classical fluids. I. Thermodynamical properties of Lennard-Jones molecules.
- [29] S. Nosé, J. Chem. Phys. **81**, 511 (1984).
A unified formulation of the constant temperature molecular-dynamics methods.
- [30] S. Nosé, Mol. Phys. **57**, 187 (1986).
An extension of the canonical ensemble molecular-dynamics method.
- [31] H. Amekura *et al.*, Phys. Rev. Mater **2**, 096001 (2018).
Vaporlike phase of amorphous SiO₂ in not a prerequisite for the core/shell ion tracks or ion shaping.
- [32] P. Kluth, R. Giulian, D. J. Sprouster, C. S. Schnohr, A. P. Byrne, D. J. Cookson, M. C. Ridgway, Appl. Phys. Lett. **94**, 113107 (2009).
Energy dependent saturation width of swift heavy ion shaped embedded Au nanoparticles.
- [33] G. Rizza, M.C. Ridgway.
Chapter 4: Ion shaping of nanoparticles in Ion Beam modification of Solids, in *Ion Beam Modification of Solids* Springer Ser. Surface Sc., Vol. 61, Werner Wesch and Elke Wendler (Eds) (2016).
- [34] Aleksi Leino, 'Elongation of nanoclusters by swift heavy ions', MSc thesis, University of Helsinki 2011.

Figure Captions

Figure 1: Scanning transmission electron microscope HAADF images of gold NPs embedded into silica: (a) as initially prepared; after vertical swift heavy irradiation at fluences of (b) $5 \times 10^{13} \text{ cm}^{-2}$, (c) $1 \times 10^{14} \text{ cm}^{-2}$ and (d) $5 \times 10^{14} \text{ cm}^{-2}$.

Figure 2: 3DTS simulation. Time evolution of a) the electronic and b) lattice temperature of a 15 nm Au NP in the silica matrix. c) Time evolution of the lattice temperature at different positions ($x=0.5 \text{ nm}, y=0, z$) along the incident-ion direction (Oz). The initial time corresponds to the impact of the incident ion. The system geometry is shown in the inset; the coordinate origin is located at the center ($x=0, y=0, z=0$) of the NP of radius r_p . Each position in the matrix is given by the distance measured from the NP surface, $z-r_p$.

Figure 3: 3DTS simulation. Time evolution of the lattice temperature in the gold NP for different diameters ($d = 2 r_p = 12, 16, 20, \text{ and } 24 \text{ nm}$) considering an incident ion passing through the NP center. The initial time corresponds to the impact of the incident ion. Each graph yields the temperature at four different positions ($x=0.5 \text{ nm}, y=0, z$) from the NP center ($x=0, y=0, z=0$) toward its surface, along the incident-ion direction (Oz). For the system geometry, see inset of Fig. 1.

Figure 4: MD evolution of the normalized volume, V/V_0 , of a 4 nm diameter NP for different heating times (computational details are given in section II.C). V_0 is the initial volume of the NP. The instantaneous heating (blue full line) is a reference for comparison purposes. The two straight dashed lines allow the determination of the time required for the complete expansion of the NP.

Figure 5: Expansion time of the NP as a function of its size. The red crosses are direct MD results, obtained as in Fig. 4, and used to establish a linear law (black line).

Figure 6: Evolution of the morphology of a NP, with a 16 nm initial diameter, irradiated by SHI up to the steady state. The arrows indicate the incident-ion direction.

Figure 7: a) Phenomenological simulation for irradiated gold NPs with initial diameters ranging from 17 to 26 nm (full circles). The evolution of each NP with the number of incident ions is shown; the numbers 1, 9 and 19 are explicitly indicated. b) NP length, L , as a function of the NP width, W , for Au-SiO₂ NPs of different initial diameters irradiated by Au ions of 185 MeV at different fluences [32].

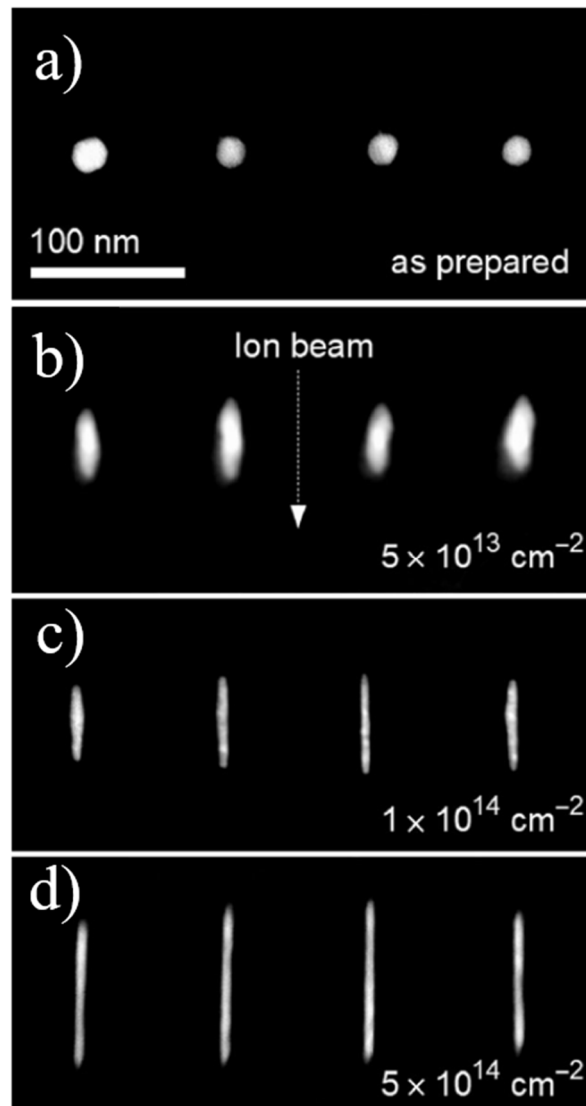


Figure 1

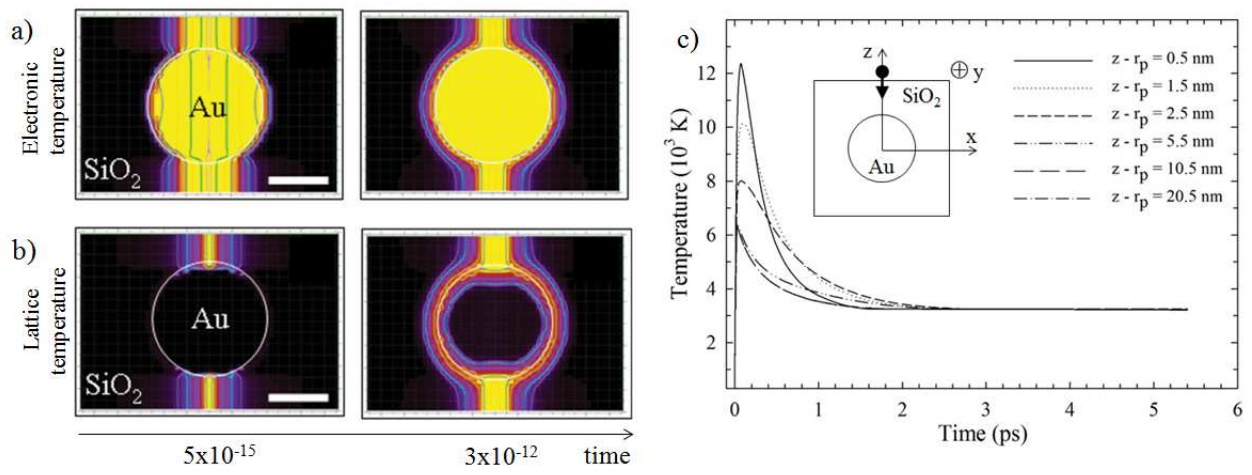


Figure 2

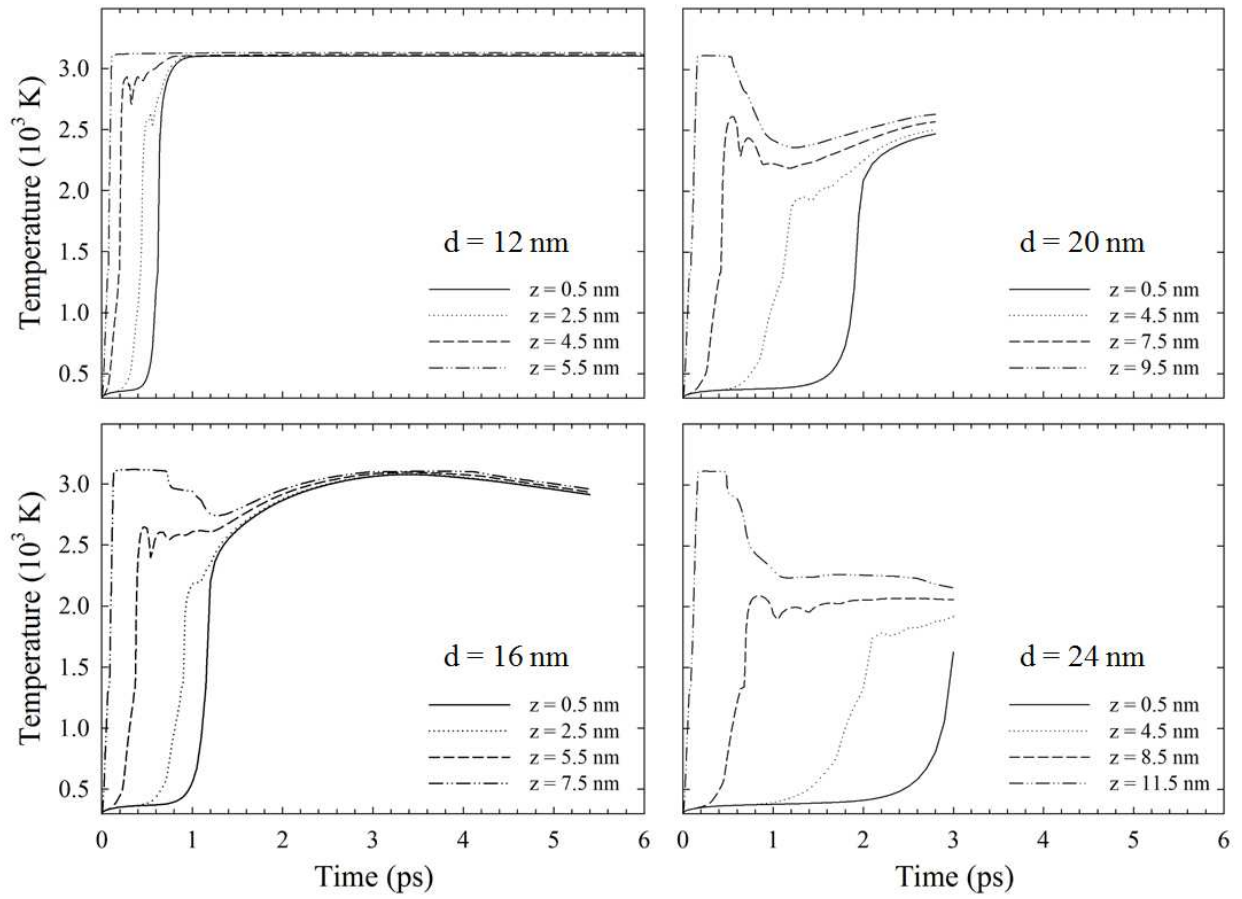


Figure 3

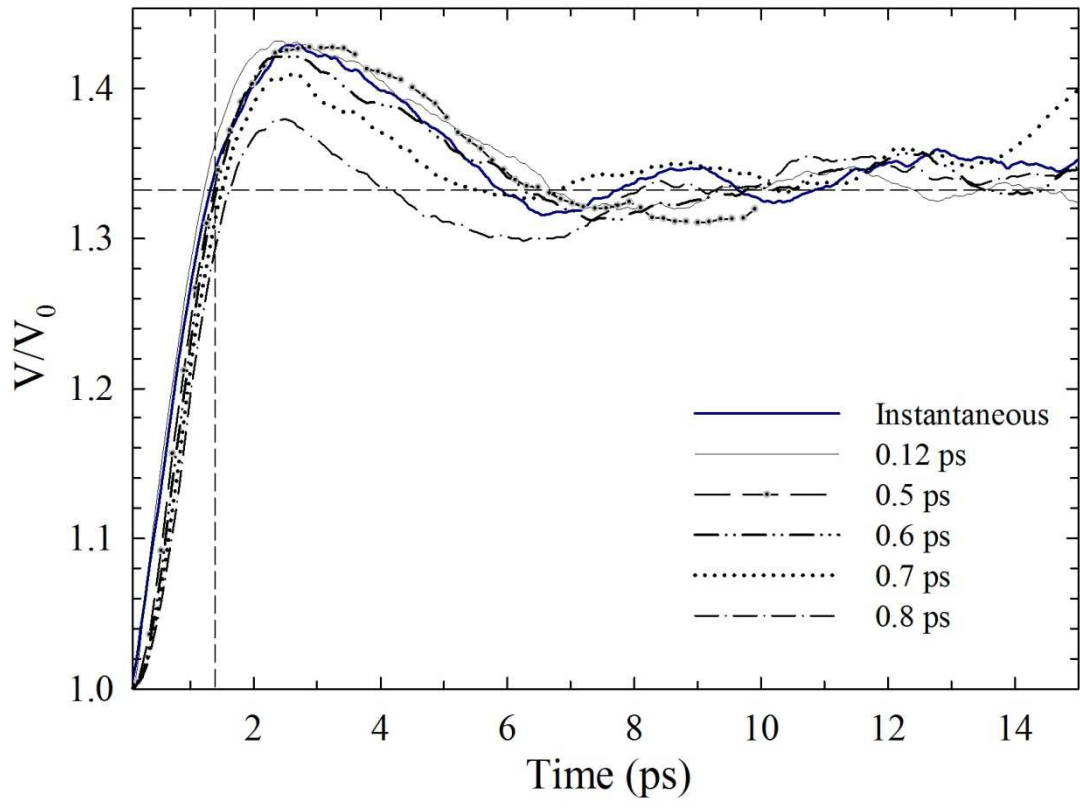


Figure 4

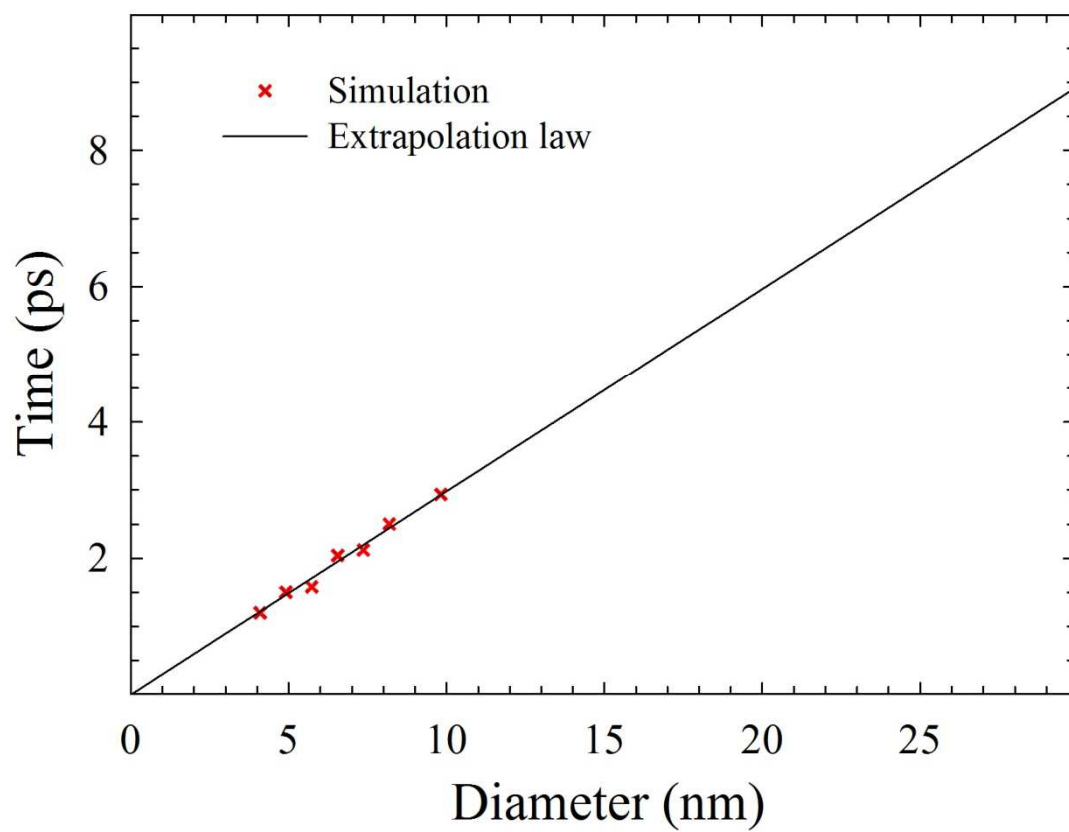


Figure 5

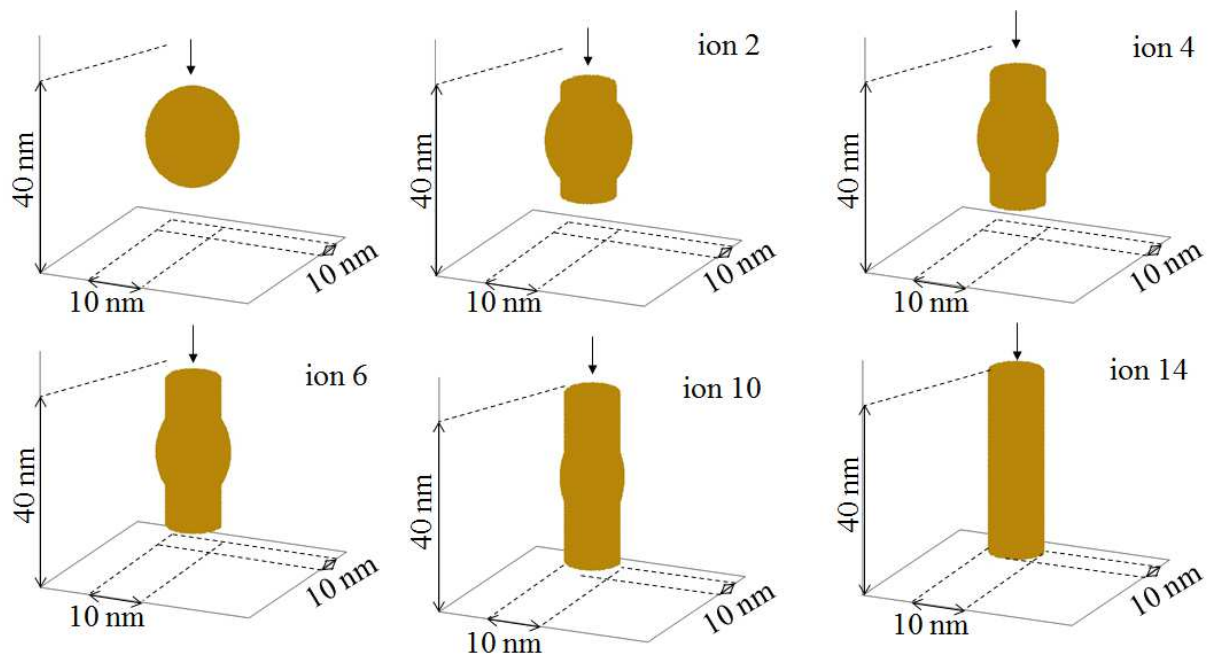


Figure 6

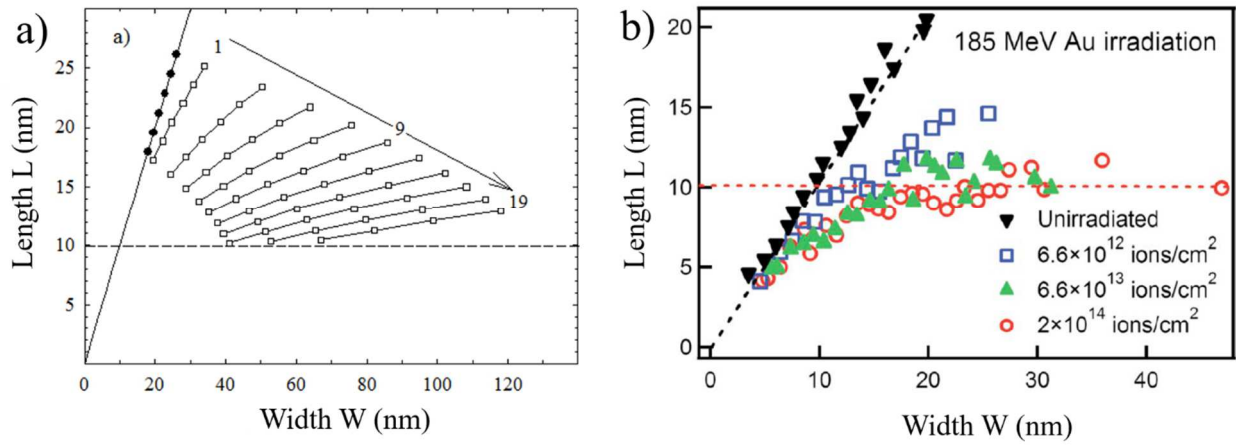


Figure 7